ACS Energy LETTERS

http://pubs.acs.org/journal/aelccp

LETTER

Tuning of the Contact Properties for High-Efficiency Si/PEDOT:PSS Heterojunction Solar Cells

Zhenhai Yang,[†] Pingqi Gao,*[,†] Jian He,[†] Wenchao Chen,[‡] Wen-Yan Yin,[‡] Yuheng Zeng,[†] Wei Guo,[†] Jichun Ye,*[,†] and Yi Cui*[,§]

[†]Ningbo Institute of Material Technology and Engineering, Chinese Academy of Sciences, Ningbo 315201, China

[‡]College of Information Science and Electronic Engineering, Zhejiang University, Hangzhou 310027, China

[§]Department of Material Science and Engineering, Stanford University, Stanford, California 94305, United States

ABSTRACT: Heterojunction solar cells (HSCs) featuring half and full contact of poly(3,4-ethylenedioxythiophene):polystyrene (PEDOT:PSS) with pyramid-textured silicon (Si) were thoroughly compared via simulations and experiments, and the following conclusions have been reached: (1) The insufficient electrical passivation inherent to the half contact results in enormous decline in short-circuit current density (J_{sc}) and open-circuit voltage (V_{oc}). (2) For the full-contact HSCs, J_{sc} is mainly dependent on the recombination at the rear interface. With tuning of the contact properties from both sides, calculated (experimental) efficiencies of 14.46%/16.89% (13.94%/16.21%) for the half-/full-contact HSCs were finally obtained. A superior power conversion efficiency (PCE) over 21% is further predicted by considering more optimal contact resistance as well as doping concentration of Si. Our findings clarify why textured-Si/PEDOT:PSS HSCs show V_{oc} and PCE that are inferior to those of planar counterparts in previous reports and further suggest a pathway to fully explore the efficiency potential of Si/PEDOT:PSS hybrid solar cells.

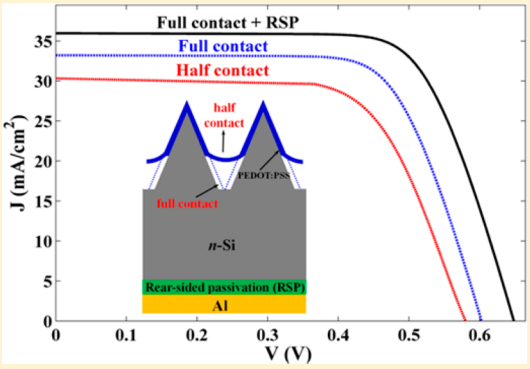

Recently, the concept of carrier-selective contacts that were previously explored for organic devices has received much interest for application in crystalline silicon solar cells.[1−11] Approaches utilizing molybdenum oxide (MoO_x),[8,9] poly(3,4-ethylenedioxythiophene):polystyrene (PEDOT:PSS),[10,11] etc. as hole-transporting layers to form high-quality hole-selective contacts with *n*-type crystalline silicon (*n*-Si) were successfully demonstrated. This kind of silicon heterojunction solar cell (HSC) relies on interface band offsets rather than conventional high-temperature doped *p*−*n* junctions to realize high-efficiency photovoltaic (PV) devices. Elimination of the need for a doping process is expected to break a number of inherent limitations of parasitic optoelectronic losses, relatively complicated fabrication processes, etc., endowing Si-based PV devices with more progressive increments in efficiency promotion and cost reduction. In terms of the Si/PEDOT:PSS HSCs, additional advantages of solution-processed fabrication procedures and easy-to-tune contact properties are also realized.[11] Through facile spin-coating of the aqueous PEDOT:PSS solution on the *n*-Si substrate followed by a low-temperature (~130 °C) annealing treatment, many groups have reported Si/PEDOT:PSS HSCs with power conversion efficiency (PCE) over 13%.[12−17] However, the efficiency is still far from satisfactory in order to be a competitive PV technology.

As is well-known, the efficiency of a solar cell is determined by the product of open-circuit voltage (V_{oc}), short-circuit current density (J_{sc}), and fill factor (FF). Contact resistance down to 0.5 Ω·cm^2 inherent to a Si/PEDOT:PSS solar cell has been measured previously, indicating FF may not be a constraint for high efficiency.[18] Meanwhile, the Si base is the only effective absorber; therefore, its light-harvesting capability can be fully boosted by utilizing advanced light-trapping designs.[19−25] Thus, the upper limit of J_{sc} for Si/PEDOT:PSS solar cells can also be clearly predicted. It follows therefore that the V_{oc} becomes a vital factor for the final efficiency. Schmidt et al. experimentally acquired a quite high level of passivation on high-resistance *n*-Si substrate (~8.9×10^{13} cm^{-3}) with double-sided PEDOT:PSS coatings, predicting a theoretical photovoltage of around 700 mV.[26] Ideally, contacting PEDOT:PSS with Si may not cause Fermi level pinning; thus, the large offset in conduction band will result in a sufficiently high self-built

Received: January 6, 2017
Accepted: February 2, 2017
Published: February 2, 2017

DOI: 10.1021/acsenergylett.7b00015
ACS Energy Lett. 2017, 2, 556−562

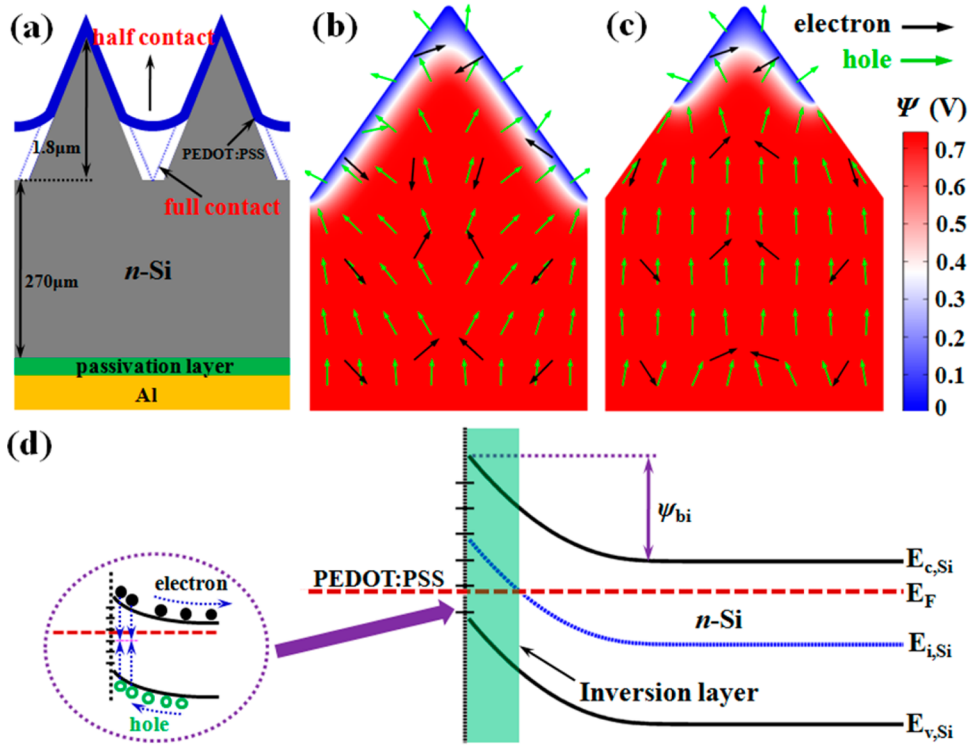

Figure 1. (a) Schematic diagram of Si/PEDOT:PSS HSCs with front surface-texturing of pyramids. The cross-sectional potential distributions as well as carrier flux [i.e., electron (black arrows) and hole (green arrows)] on the front surface for full (b) and half (c) contact. (d) Energy band diagram near the silicon interface.

electrical potential for electron rejection.[27] The strong electrical field near the Si/PEDOT:PSS interface is believed to induce accumulations of holes near the *n*-Si surface and to produce an inversion layer, which is rationally interpreted as a driving force that abets the hybrid device similar to a common p^+n junction.[27−29] This should lead to much higher V_{oc} because it is governed by the quasi-Fermi level splitting of electrons and holes in the whole device under illumination, which can be enhanced by elevating the work function of PEDOT:PSS, increasing the doping level of the Si substrate, suppressing the bulk recombination, as well as minimizing the unpassivated interfacial electronic states. Designs strategies focusing on the former two aspects are straightforward, and the bulk recombination can be neglected for the high-quality *n*-Si substrate with moderate doping concentration;[30] the interface recombination between Si/PEDOT:PSS and rear-electrode/Si are therefore the dominate factors restricting V_{oc}. It is thus meaningful to make a thorough performance evaluation from the recombination rate viewpoint on Si/PEDOT:PSS HSCs, aiming for more rational design and management. Meanwhile, the reported Si/PEDOT:PSS HSCs show typical V_{oc} less than 630 mV for planar structure and below 600 mV for devices with advanced Si texturing, mainly because of the significant recombination arising from the poorly passivated junction.[31−33]

To date, the far from optimal interface preparation led to unsatisfactory efficiencies. Therefore, new strategies are needed to improve the junction quality and performances of Si/PEDOT:PSS HSCs.

In this Letter, we focus particularly on the Si/PEDOT:PSS HSCs with state-of-the-art pyramidal surface textures and investigate the optoelectronic performances under different interface recombination velocities, contact resistances, and doping concentrations of Si substrate. To mimic the practical conditions, two typical contact configurations between Si-pyramids and PEDOT:PSS (i.e, half contact and full contact) were fully characterized via well-designed experiments and simulations for both external quantum efficiency (EQE) responses and current density−voltage (J−V) curves. The detailed results indicate that (1) the enormously degraded electrical performances (including J_{sc} and V_{oc}) of half-contact HSCs are mainly related to the severe recombination in the unpassivated interface; (2) for the full-contact HSCs, J_{sc} is sensitive/insensitive to the rear/front interface, but V_{oc} is dependent on the quality of both front Si/PEDOT:PSS and rear Si/electrode interfaces; (3) the full contact produces a large decrease of front surface recombination velocity from 300 to 100 cm/s, resulting in a significant efficiency boost from 13.94% to 16.21%, and a superior efficiency over 18% is possible for moderately doped Si substrate ($\sim 2 \times 10^{15}$ cm^{-3}) if the double-sided passivation can be improved with the recombination velocity less than 10 cm/s. Finally, by fully considering the combined actions from modifications of passivation, substrate doping concentrations, and contact resistances, a potential efficiency beyond 21% was further predicated, imposing a certain significance to constructing high-efficiency Si/PEDOT:PSS HSCs.

Figure 1a shows the schematic diagram used for simulation, which is composed of a 80 nm PEDOT:PSS film, front-side textured *n*-Si substrate (thickness, 270 μm; doping concentration, $N_d = 2 \times 10^{15}$ cm^{-3}; electrical conductivity, $\rho \sim 2.3$ Ω·cm), rear passivation layer, and aluminum (Al) electrode. Note that the front electrode of silver grids is not shown in Figure 1a for clarity. In order exactly mimic the experimental conditions, two types of contacts between PEDOT:PSS thin film and the Si-pyramid arrays are defined according to the scanning electron microscopy (SEM) micrographs (please refer to

DOI: 10.1021/acsenergylett.7b00015
ACS Energy Lett. 2017, 2, 556−562

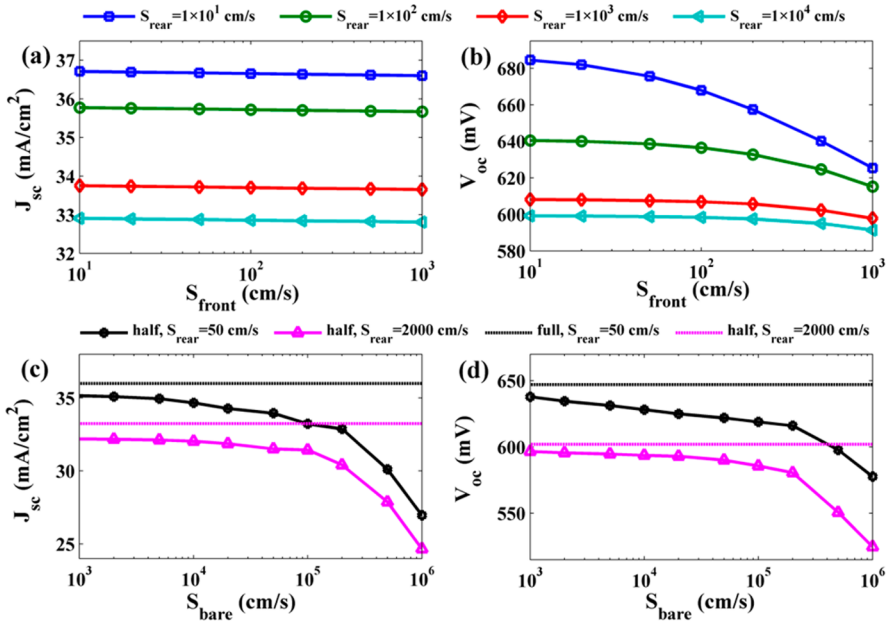

Figure 2. (a) J_{sc} and (b) V_{oc} as a function of S_{front} for the full-contact HSCs, in which four typical rear recombination velocities were shown, i.e., $S_{rear} = 1 \times 10^1$, 1×10^2, 1×10^3, and 1×10^4 cm/s. (c) J_{sc} and (d) V_{oc} versus S_{bare} for the half-contact HSCs under $S_{front} = 100$ cm/s, $S_{rear} = 50$, and 2000 cm/s. The full-contact values (black dotted line for $S_{rear} = 50$ cm/s and magenta dotted line for $S_{rear} = 2000$ cm/s) are also inserted for reference.

Figure 3c,d). The period and height of the pyramid arrays are set as 3 and 1.8 μm, respectively. The blue solid- and dotted-regions represent the half- and full-contact situations, whereas the ratio of uncovered/entire area for the half-contact case is fixed at 0.5.

To comprehensively understand the difference between full and half contact, the cross-sectional potential distributions as well as the energy band diagram are illustrated in Figure 1b–d. It is apparent that though the interface contact (i.e., half or full contact) is not sensitive to the maximum value of potential (i.e., built-in potential, ψ_{bi}), it has a decisive impact on potential distribution as well as the effective area for carrier collection. The rigorous calculations show that in thermal equilibrium, the thickness of the inversion and depletion layers and ψ_{bi} are 218 and 680 nm and 703 mV, respectively, under the doping concentration of Si substrate of 2×10^{15} cm^{-3} and the work function of PEDOT:PSS of 5.0 eV. When these results are combined with the energy band diagram in Figure 1d, we can find that the interface contact does not change the defect state density of related contact interface, but it heavily affects the effect of the electrical passivation, when we assume PEDOT:PSS has no chemical passivation for Si surface. Although the electric field intensity that is dominated by ψ_{bi} is unchanged for the two types of contacts under the fixed doping concentration of Si substrate and the work function of PEDOT:PSS, the area that was not covered by PEDOT:PSS is hardly passivated by the electrical field, and there is no doubt that the interfacial recombination probability increases. Therefore, the essential difference for the two contacts is the size of the electrical passivation region, rather than the change in electric field intensity.

We first focus on the electrical responses (i.e., J_{sc} and V_{oc}) of the full-contact HSCs, as shown in Figure 2ab. Here, one must note that in our simulation, the bulk lifetime of Si substrate reaches 3 ms; therfore, the bulk recombination including the Shockley–Read–Hall (SRH), radiative, and Auger recombination is very small, and the surface recombination is the main loss source in the HSCs.[29] By careful observation, we can determine the following: (1) The front recombination velocity (S_{front}) has a very limited influence on the J_{sc}, which is because only a small number of electron–hole pairs generated in the depletion region and the ψ_{bi} close to the front interface can effectively block the electron (majority carrier) from diffusing into top interface, leading to less recombination even under a condition of large S_{front}. (2) The rear recombination velocity (S_{rear}) has a strong impact on the J_{sc}, owing to plenty of collective holes on the rear interface. As a result, J_{sc} increased from 32.85 to 36.65 mA/cm^2 when regulating S_{rear} from 1×10^4 to 1×10^1 cm/s under $S_{front} = 100$ cm/s. (3) S_{rear} dominates the V_{oc}, but it is not the only factor. (4) S_{front} is rather sensitive/insensitive to the V_{oc} when the S_{rear} is small/large enough, e.g., when $S_{rear} = 1 \times 10^1$ (1×10^4) cm/s, V_{oc} decreased from 684 (599) to 625 (591) mV as S_{front} increased from 1×10^1 to 1×10^3 cm/s with the decrement of 59 and 8 mV, respectively. Our theoretical simulation and analysis indicate that if the rear interface is well-passivated ($S_{rear} < 1 \times 10^2$ cm/s), it is easy to further increase the V_{oc} but difficult to increase J_{sc} by optimizing the front interface; in contrast, if the rear interface is poorly passivated ($S_{rear} > 1 \times 10^4$ cm/s), it is unrealistic to expect substantial improvements on J_{sc} or V_{oc} only through regulating the front interfacial passivation.

Next, we consider incomplete contact (half contact) of PEDOT:PSS and Si, which may be ubiquitous in preparation of Si/PEDOT:PSS cells on heavily textured Si surface. Here, the recombination velocity of uncovered interface (S_{bare}) ranges from 1×10^3 to 1×10^6 cm/s because the recombination of the uncovered region is much bigger than that of the coated area. Panels c and d of Figure 2 display the J_{sc} and V_{oc} versus S_{bare} of the uncovered interface, respectively, where full-contact systems are plotted as well. In this study, in order to correspond to our experimental results, two sets of typical simulated parameters (i.e, $S_{front} = 100$ cm/s, $S_{rear} = 50$ cm/s and $S_{front} = 100$ cm/s, S_{rear}

DOI: 10.1021/acsenergylett.7b00015
ACS Energy Lett. 2017, 2, 556–562

= 2000 cm/s) were chosen. It is observed from the figures that the values of J_{ph} and V_{oc} show a strong dependence on S_{bare}, specially when $S_{bare} > 1 \times 10^5$ cm/s, e.g., when $S_{bare} = 2 \times 10^5$ cm/s, the J_{ph} (V_{oc}) declined from 35.99/33.24 mA/cm^2 (647/602 mV) to 32.87/30.41 mA/cm^2 (616/580 mV) at S_{rear} = 50/2000 cm/s. Therefore, the half contact degraded the performance of HSCs on both J_{sc} and V_{oc} when the rear passivation was good or poor.

For further insight into the performance responses of HSCs, we compared the simulated and experimental J_{sc} and V_{oc} as shown in Figure 3a,b, in which three typical HSCs were

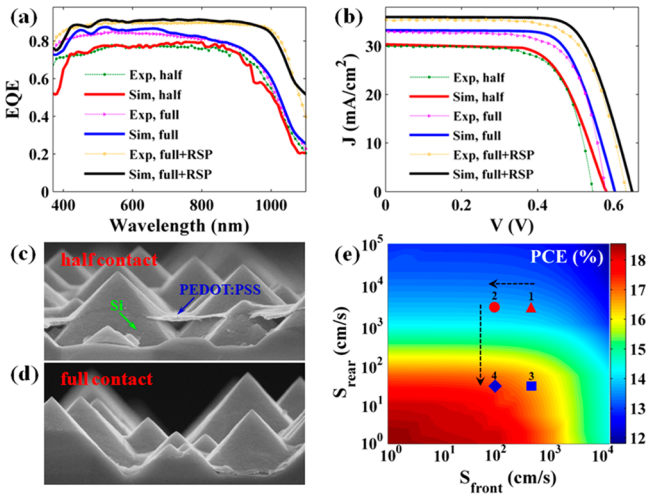

Figure 3. Experimental (thin dotted line) and simulated (bold solid line) (a) EQE spectra and (b) $J-V$ characteristics of the PEDOT:PSS/n-Si HSCs, where the half contact, full contact, and full contact with RSP layer are presented. (c, d) SEM cross-sectional micrographs of PEDOT:PSS/textured-Si stacks for the half and full contact. (e) Simulated PCE versus S_{front} and S_{rear} for the full-contact HSCs.

considered, i.e., half contact, full contact, and full contact with rear-sided passivation (RSP) layer. Moreover, the SEM micrographs of Si-pyramids/PEDOT:PSS stacks for the half and full contact are presented in panels c and d of Figure 3, respectively. Here, the half or full contacts represent the rear interface is nonpassivated (n-Si/Al contact), and the full contact with passivation layer means the rear interface is passivated by a-Si:H(i)/a-Si:H(n) layers. According to Table 1, the a-Si:H(i)/a-Si:H(n) passivation produces a rear surface recombination velocity of around 50 cm/s (measured by minority carrier lifetime tests), while the derived front surface recombination velocities are about 100 and 300 cm/s for the full- and half-contact, respectively. To fit the experimental situation, the recombination velocities in the numerical calculation are chosen as follows: S_{rear} = 2000 cm/s, $S_{bare} = 2 \times 10^5$ cm/s for half contact, and S_{rear} = 2000/50 cm/s for full contact without/with RSP layer, respectively, where the front recombination velocity S_{front} was regarded as a constant (100 cm/s), assuming that the PEDOT:PSS has a similar passivation effect on the textured-Si surface.

Figure 3a,b provides a detailed comparison of EQE spectra and $J-V$ curves of the HSCs for both experimental and simulated cases with the half-contact, full-contact, and full-contact with RSP layer configurations. It is apparent that the simulated results are in good agreement with experimental ones (the slight deviations mainly result from the difference in optical reflectivity). Figure 3a indicates that the EQE of full-contact HSCs overwhelms the half one in full spectrum (especially at short waveband), leading to an increased J_{sc} (i.e., from 30.41/30.30 mA/cm^2 to 33.24/32.60 mA/cm^2 for the simulation/experiment as shown in Table 1). The main reason for the degraded performances for the half-contact HSCs is inherent to the partially covered front interface uncovered by PEDOT:PSS that cannot be passivated by the electric field (as shown in Figure 1b,c), resulting in the gathering of a mass of minority/majority carriers and thus a huge recombination loss. The enhanced EQE is wavelength-dependent (i.e., as the wavelength increases, the enhanced EQE displays a downward trend), which is because (i) at short wavelengths, the photon-generated carriers numerously distributed near the front interface, so the increased minority carrier concentration of the uncovered region leads to severe recombination; (ii) at long-wavelengths, the internal quantum efficiency (IQE) of HSCs rapidly decayed for the two systems because of the poor passivation of rear side interface; thus, the EQE of the full-contact case has no obvious superiority in contrast with the half-contact case. Furthermore, with the help of the RSP layer, EQE with average values of about 0.9 at wavelengths from 400 to 1000 nm increased continuously, yielding a prodigious J_{sc} of 35.99/35.40 mA/cm^2 for the simulation/experiment. This advance is dominated by the improved junction quality when checking the reflection spectra. The corresponding $J-V$ curves are presented in Figure 3b. Careful observation shows that V_{oc} is 580/557 mV (half contact), 602/577 mV (full contact), and 647/634 mV (full contact with RSP) for the simulation/experiment. The RSP layer that congenitally reduces the recombination of the rear-side interface not only contributes to split Fermi level, resulting in enormous enhancement for V_{oc},

Table 1. Parameter Lists Including Built-in Potential (ψ_{bi}), Thickness of Inversion and Depletion Layers, J_{sc}, V_{oc}, PCE, S_{front}, and S_{rear} under $N_d = 2 \times 10^{15}$ cm^{-3} and 1×10^{17} cm^{-3}

				J_{sc} (mA/cm^2)		V_{oc} (mV)		PCE (%)		S_{front} (cm/s)	S_{rear} (cm/s)
N_d (cm^{-3})	ψ_{bi} (mV)	inversion/depletion layer (nm)	contact	sim	exptl	sim	exptl	sim	exptl	(measure)	(measure)
2×10^{15}	703	218/680	half	30.41	30.30	580	557	12.25	11.70	300	–
			full	33.24	32.60	602	577	13.88	13.10	100	–
			half with RSP	32.87	32.20	616	609	14.46	13.94	300	50
			full with RSP	35.99	35.40	647	634	16.89	16.21	100	50
1×10^{17}	804	28/103	full with RSP	35.40		690		19.08 (R_c = 2.5 Ω·cm^2); 21.30 (R_c = 0.5 Ω·cm^2)		100 (assume)	50 (assume)

DOI: 10.1021/acsenergylett.7b00015
ACS Energy Lett. 2017, 2, 556−562

but also promotes the efficiency of carrier collection for the double-sided interfaces, leading to the great improvement in J_{sc}.

To intuitively reflect the impact of interface passivation on performances of HSCs, we illustrate the PCE as functions of rear and front recombination velocities (S_{rear} and S_{front}) under the full-contact case, as shown in Figure 3e. Unsurprisingly, the value of the PCE has strong dependences on both S_{rear} and S_{front}, showing that the interface passivation plays very crucial roles in determining the output performances of the HSCs. The conversion efficiencies of full contact (point 2, red circle, S_{front} = 100 cm/s, and S_{rear} = 2000 cm/s) and full contact with RSP layer (point 4, blue rhombus, S_{front} = 100 cm/s, and S_{rear} = 50 cm/s) are marked in the figure with the values of 13.88% and 16.89%, respectively, which is well-matched with the experimental results (i.e., 13.10% and 16.21% for the two systems). Moreover, the contacts with poor passivation are also presented in the figure (i.e., point 1, red triangle, S_{front} = 300 cm/s, S_{rear} = 2000 cm/s and point 3, blue square, S_{front} = 300 cm/s and S_{rear} = 50 cm/s). In the fabrication approach, we do not want to use a-Si:H(i)/a-Si:H(n) layers as RSP to passivate the rear side of n-Si base because it is slightly conflicting with the ultimate idea of being dopant-free. However, if the rear side passivation is very bad, one may not see the performance changes from partial contact to full contact in between PEDOT:PSS and structured-Si, because in that case the rear-side recombination is dominant. As can be seen from the plot in Figure 3e, the PCE can be changed at the same level only from point 1 to point 2, not from point 1 to point 4, if lacking the rear-sided a-Si:H(i)/a-Si:H(n) passivating layers, under which condition S_{rear} is almost constant. Our findings first clarified why textured-Si/PEDOT:PSS hybrid solar cells show inferior V_{oc} and efficiency over planar counterparts in previous reports and further suggest a pathway to fully explore the efficiency potential. With the full-contact Si/PEDOT:PSS heterointerface at the front surface and medium quality of passivation by the a-Si:H(i)/a-Si:H(n) at the rear surface, a final efficiency of 16.21% for this conventional Si/PEDOT:PSS HSC was achieved. Moreover, the results reveal that the PCE of full-contact HSCs can be further improved (over 18%) by reducing the interface recombination with recombination velocity less than 10 cm/s.

Finally, we investigate the roles of the substrate doping concentration and the contact resistance of the HSCs at the constant interface recombination velocities (i.e., S_{front} = 100 cm/s and S_{rear} = 50 cm/s) for the full-contact condition. Figure 4a plots the V_{oc} and PCE versus doping concentration (N_d) of Si substrate, where the detailed electrical parameters for different N_d (including carrier mobility and bulk lifetime, etc.) can be found in previous publications.[33] The blue dashed line (red solid line) in Figure 4a shows that the V_{oc} (PCE) steadily increases from 634 mV (16.38%) to 690 mV (19.08%) with increasing N_d, i.e., from 1×10^{15} ($\rho \sim 4.5$ Ω·cm) to 1×10^{17} cm^{-3} ($\rho \sim 0.085$ Ω·cm). With the increase of N_d, the Fermi level of n-Si moves closer to its conduction band, leading to a sharp increase in ψ_{bi} and thus V_{oc} of the related HSCs (here, we did not consider the change in interface state). Moreover, under the condition of uniform passivation, there is a correspondence relationship between PCE and V_{oc}. That means the significant rise of PCE mostly relates to the boost in V_{oc}, regardless of the slightly declining J_{sc}.

In addition, as mentioned above, contact resistance is a vital factor to restrict FF as well as PCE; therefore, it is necessary to investigate the electrical responses of HSCs (i.e., FF and PCE) in terms of the contact resistance as shown in Figure 4b, where

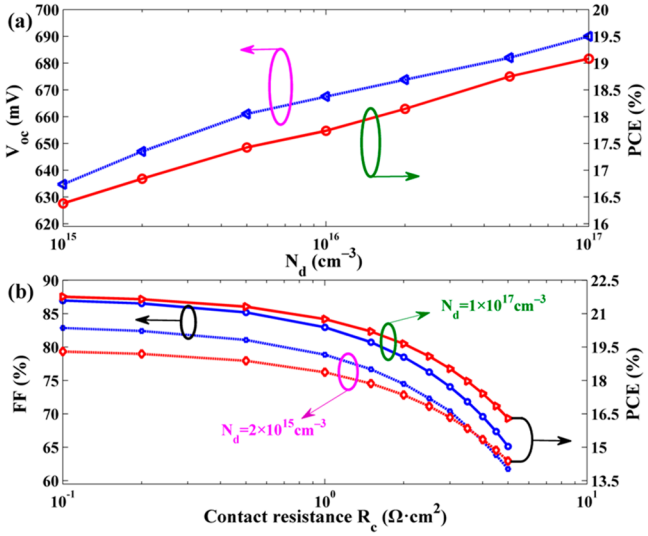

Figure 4. (a) V_{oc} (blue dotted line) and PCE (red solid line) as a function of doping concentration of Si substrate (N_d) for the full-contact HSCs under the constant recombination, i.e., S_{front} = 100 cm/s and S_{rear} = 50 cm/s. (b) FF and PCE versus contact resistance R_c under $N_d = 2 \times 10^{15}$ cm^{-3} and 1×10^{17} cm^{-3}.

two typical N_d values (i.e., 2×10^{15} cm^{-3} and 1×10^{17} cm^{-3}) were considered. The following are observed from the figure: (1) With increasing contact resistance, the values of FF and PCE for the two doping concentrations, N_d, are primarily monotonically decreased. (2) The device with $N_d = 1 \times 10^{17}$ cm^{-3} shows a FF that is much higher than that of $N_d = 2 \times 10^{15}$ cm^{-3} under the same contact resistance. (3) The PCE for the two systems can reach 19.29% and 21.30% when the contact resistance reduces to 0.5 Ω·cm^2. Therefore, on the basis of high-quality passivation, the pyramid-textured Si/PEDOT:PSS HSCs have a huge potential for realizing an efficiency as high as that of commercialized Si PV technology.

In summary, we theoretically and experimentally present a significant evaluation on pyramid-structured Si/PEDOT:PSS HSCs by addressing EQE responses, $J-V$ curves, and PCE. In particular, two typical contacts (i.e, half contact and full contact) were considered to reveal the influence of interface properties on photoelectric performances of this kind of HSC. For the half contact, the uncovered region without electrical passivation results in severe interface recombination, leading to the huge decline in J_{sc} and V_{oc} compared with full-contact case. Thus, the PCE value decreases from 13.88%/13.10% (full contact) to 12.25%/11.70% (half contact) for the simulation/experiment case. The underlying improvement in PCE (i.e., 16.89% for experiment and 16.21% for simulation) for full-contact HSCs can be realized through cooperation with the rear-sided a-Si:H(i)/a-Si:H(n) passivation layer. Moreover, our results predict a superior PCE beyond 18% by the high-quality passivation with the double-sided recombination velocities less than 10 cm/s. When the substrate doping concentrations and contact resistances are modified, a remarkable PCE of Si/PEDOT:PSS HSCs with a value of 21.30% can be further asserted, showing a huge potential to compete with conventional PV technology.

METHODS

Experimental Methods. In this experiment, one-side polished n-type Si wafers (CZ, 270 μm, 1−3 Ω·cm, i.e., N_d = 1.5−4.8 ×

DOI: 10.1021/acsenergylett.7b00015
ACS Energy Lett. 2017, 2, 556−562

10^{15} cm^{-3}) are prepared. The fabrication process of Si/PEDOT:PSS HSCs with rear a-Si:H layers is as follows: (1) Random pyramid structures were textured on double sides of the wafer by immersion in NaOH (2.5%) and isopropanol (1.25%) solutions for 10 min, and then the rear side was polished in HF:HNO_3 solution with a volume ratio of 1:20. (2) A standard RCA cleaning and a dilute HF dip was implemented. (3) A 5 nm thick intrinsic hydrogenated amorphous silicon [a-Si:H(i)] film was deposited on the back side of the wafers by plasma-enhanced chemical vapor deposition (PECVD, MVSystems, United States). (4) A 10 nm thick highly doped a-Si:H(n) layer was subsequently deposited as the surface field layer. (5) A 200 nm Al layer was thermally evaporated at the rear side of a-Si:H. (6) A PEDOT:PSS (PH1000) solution mixed with 7 wt % ethylene glycol and 0.25 wt % Triton-100 (from Aldrich) was spin-coated on the random pyramid surface with a thickness of about 80 nm; the sample was then annealed at 135 °C to remove the solvents to form a highly conductive p-type organic thin film. (7) A Ag film (300 nm) was subsequently thermally evaporated on top of the PEDOT:PSS layer. Note that the uniform PEDOT:PSS layer can rarely be conformably coated on the Si pyramids because of its polymeric characteristics; we thus defined the Si/PEDOT:PSS HSCs fabricated by procedures 1−7 as half-contact HSCs. A full-contact device was achieved by a postfabrication coating of a water-insoluble pathalic acid ester, diethyl phthalate (DEP), which is dissolved in acetone with mass fraction of 50% and spin-coated upon the PEDOT:PSS layer in the as-fabricated device.[34]

The surface recombination velocities are deduced by the effective minority carrier lifetimes, which is measured by a Sinton WCT-120 instrument based on the transient photoconductance (TPCD) method.[11] The objective of quantifying the resultant front and rear surface recombination velocity (S_{front} and S_{rear}) was realized by using the symmetrical pyramid structures coated with PEDOT:PSS and a-Si:H passivated structures.[31] The corresponding results are listed in Table 1.

Simulation Methods. The photoelectric simulations of Si/PEDOT:PSS HSCs were implemented by using finite element method, in which the optical (electrical) simulation is obtained by solving Maxwell's (drift-diffusion and Poisson) equations. In this simulation, we assume ideal textured pyramids with a periodic configuration, so the perfect electric/magnetic conductor boundaries (i.e., optically periodic) and semiconductor symmetric conditions (i.e., electrically periodic) can be used. In the optical model, the perfectly matched layers were employed on the front- and rear-side region to restrict the calculated domain. By coupling the spatial structure with the frequency domain, the optical parameters including absorption response and electric field distribution can be easily achieved. In the electrical module, the electrical processes of HSCs, including carrier transport, recombination, and collection, are based on the carrier generation in the optical model under the source of air mass 1.5G; thus, the stabilized distributions of photoelectrical parameters can be well addressed. In addition, the photoelectric parameters used in the simulation (include the material refractive index, electron and hole mobility, carrier lifetime, coefficients of various kinds of carrier recombination, material bandgap, etc.) can be found in previous publications.[30,35−37]

We must note that in the Si/PEDOT:PSS hybrid device, the PEDOT:PSS with a relatively high work function (~5.0 eV) serves as hole-transporting material, providing charge separation by its hole-selective nature. In this study, we treated Si/PEDOT:PSS as abrupt p^+n-heterojunction, because the transport mechanism dominating the hybrid Si/PEDOT:PSS junction is the diffusion of minority carriers in the silicon bulk and not the thermionic emission of majority carriers at the interface.[26]

AUTHOR INFORMATION

Corresponding Authors

*E-mail: gaopingqi@nimte.ac.cn.
*E-mail: jichun.ye@nimte.ac.cn.
*E-mail: yicui@stanford.edu.

ORCID

Pingqi Gao: 0000-0002-6424-4835

Notes

The authors declare no competing financial interest.

ACKNOWLEDGMENTS

This work was financially supported by Zhejiang Provincial Natural Science Foundation (LR16F040002), National Natural Science Foundation of China (61674154, 61404144, 61431014, 61504121), International S&T Cooperation Program of Ningbo (2015D10021), and Major Project and Key S&T Program of Ningbo (2016B10004, 2014B10026).

REFERENCES

(1) Jeong, S.; Garnett, E. C.; Wang, S.; Yu, Z.; Fan, S.; Brongersma, M. L.; McGehee, M. D.; Cui, Y. Hybrid Silicon Nanocone−Polymer Solar Cells. *Nano Lett.* **2012**, *12*, 2971−2976.

(2) Liu, Y.; Zhang, Z.; Xia, Z.; Zhang, J.; Liu, Y.; Liang, F.; Li, Y.; Song, T.; Yu, X.; Lee, S. T.; Sun, B. High Performance Nanostructured Silicon−Organic Quasi p−n Junction Solar Cells via Low-Temperature Deposited Hole and Electron Selective Layer. *ACS Nano* **2016**, *10*, 704−712.

(3) Tsai, M. L.; Wei, W. R.; Tang, L.; Chang, H. C.; Tai, S. H.; Yang, P. K.; Lau, S. P.; Chen, L. J.; He, J. H. Si Hybrid Solar Cells with 13% Efficiency via Concurrent Improvement in Optical and Electrical Properties by Employing Graphene Quantum Dots. *ACS Nano* **2016**, *10*, 815−821.

(4) Chen, T. G.; Huang, B. Y.; Chen, E. C.; Yu, P.; Meng, H. F. Micro-Textured Conductive Polymer/Silicon Heterojunction Photovoltaic Devices with High Efficiency. *Appl. Phys. Lett.* **2012**, *101*, 033301.

(5) Walter, M. G.; Liu, X.; O'Leary, L. E.; Brunschwig, B. S.; Lewis, N. S. Electrical Junction Behavior of Poly (3, 4-ethylenedioxythiophene) (PEDOT) Contacts to H-Terminated and CH3-Terminated p-, n-, and n^+-Si (111) Surfaces. *J. Phys. Chem. C* **2013**, *117*, 14485−14492.

(6) Subramani, T.; Syu, H. J.; Liu, C. T.; Hsueh, C. C.; Yang, S. T.; Lin, C. F. Low-Pressure-Assisted Coating Method to Improve Interface Between PEDOT:PSS and Silicon Nanotips for High-Efficiency Organic/Inorganic Hybrid Solar Cells via Solution Process. *ACS Appl. Mater. Interfaces* **2016**, *8*, 2406−2415.

(7) Chen, J. Y.; Yu, M. H.; Chang, S. F.; Sun, K. W. Highly Efficient Poly (3, 4-ethylenedioxythiophene): Poly (styrenesulfonate)/Si Hybrid Solar Cells with Imprinted Nanopyramid Structures. *Appl. Phys. Lett.* **2013**, *103*, 133901.

(8) Um, H. D.; Kim, N.; Lee, K.; Hwang, I.; Seo, J. H.; Seo, K. Dopant-Free All-Back-Contact Si Nanohole Solar Cells Using MoO_x and LiF Films. *Nano Lett.* **2016**, *16*, 981−987.

(9) Bullock, J.; Hettick, M.; Geissbühler, J.; Ong, A. J.; Allen, T.; Sutter-Fella, C. M.; Chen, T.; Ota, H.; Schaler, E. W.; De Wolf, S.; Ballif, C.; Cuevas, A.; Javey, A.; Andrés, C.; Ali, J. Efficient Silicon Solar Cells with Dopant-Free Asymmetric Heterocontacts. *Nat. Energy* **2016**, *1*, 15031.

DOI: 10.1021/acsenergylett.7b00015
ACS Energy Lett. 2017, 2, 556−562

(10) Syu, H. J.; Shiu, S. C.; Lin, C. F. Silicon Nanowire/Organic Hybrid Solar Cell with Efficiency of 8.40%. *Sol. Energy Mater. Sol. Cells* **2012**, *98*, 267−272.
(11) Sheng, J.; Fan, K.; Wang, D.; Han, C.; Fang, J.; Gao, P.; Ye, J. Improvement of the SiO_x Passivation Layer for High-Efficiency Si/PEDOT:PSS Heterojunction Solar Cells. *ACS Appl. Mater. Interfaces* **2014**, *6*, 16027−16034.
(12) He, J.; Gao, P.; Liao, M.; Yang, X.; Ying, Z.; Zhou, S.; Ye, J.; Cui, Y. Realization of 13.6% Efficiency on 20 μm Thick Si/Organic Hybrid Heterojunction Solar Cells via Advanced Nanotexturing and Surface Recombination Suppression. *ACS Nano* **2015**, *9*, 6522−6531.
(13) Zhang, Y.; Cui, W.; Zhu, Y.; Zu, F.; Liao, L.; Lee, S. T.; Sun, B. High Efficiency Hybrid PEDOT:PSS/Nanostructured Silicon Schottky Junction Solar Cells by Doping-Free Rear Contact. *Energy Environ. Sci.* **2015**, *8*, 297−302.
(14) Liu, Q.; Ishikawa, R.; Funada, S.; Ohki, T.; Ueno, K.; Shirai, H. Highly Efficient Solution-Processed Poly(3,4-ethylenedioxythiophene):Poly(styrenesulfonate)/Crystalline− Silicon Heterojunction Solar Cells with Improved Light-Induced Stability. *Adv. Energy Mater.* **2015**, *5*, 1500744.
(15) Liu, R.; Lee, S. Y.; Sun, B. 13.8% Efficiency Hybrid Si/Organic Heterojunction Solar Cells with MoO_3 Film as Antireflection and Inversion Induced Layer. *Adv. Mater.* **2014**, *26*, 6007−6012.
(16) Thomas, J. P.; Leung, K. T. Defect-Minimized PEDOT:PSS/Planar-Si Solar Cell with Very High Efficiency. *Adv. Funct. Mater.* **2014**, *24*, 4978−4985.
(17) He, J.; Yang, Z.; Liu, P.; Wu, S.; Gao, P.; Wang, M.; Zhou, S.; Li, X.; Cao, H.; Ye, J. Enhanced Electro-Optical Properties of Nanocone/Nanopillar Dual-Structured Arrays for Ultrathin Silicon/Organic Hybrid Solar Cell Applications. *Adv. Energy Mater.* **2016**, *6*, 1501793.
(18) Gogolin, R.; Zielke, D.; Lövenich, W.; Sauer, R.; Schmidt, J. Silicon Heterojunction Solar Cells Combining an a-Si:H(n) Electron-Collector with a PEDOT:PSS Hole-Collector. *Energy Procedia* **2016**, *92*, 638−643.
(19) Lin, H.; Xiu, F.; Fang, M.; Yip, S. P.; Cheung, H. Y.; Wang, Y.; Han, N.; Chan, K. S.; Wong, C. Y.; Ho, J. C. Rational Design of Inverted Nanopencil Arrays for Cost-Effective, Broadband, and Omnidirectional Light Harvesting. *ACS Nano* **2014**, *8*, 3752−3760.
(20) Gaucher, A.; Cattoni, A.; Dupuis, C.; Chen, W.; Cariou, R.; Foldyna, M.; Lalouat, L.; Drouard, E.; Seassal, C.; Roca i Cabarrocas, P.; Collin, S. Ultrathin Epitaxial Silicon Solar Cells with Inverted Nanopyramid Arrays for Efficient Light Trapping. *Nano Lett.* **2016**, *16*, 5358−5364.
(21) Zhou, S.; Yang, Z.; Gao, P.; Li, X.; Yang, X.; Wang, D.; He, J.; Ying, Z.; Ye, J. Wafer-Scale Integration of Inverted Nanopyramid Arrays for Advanced Light Trapping in Crystalline Silicon Thin Film Solar Cells. *Nanoscale Res. Lett.* **2016**, *11*, 194.
(22) Yang, Z.; Li, X.; Wu, S.; Gao, P.; Ye, J. High-Efficiency Photon Capturing in Ultrathin Silicon Solar Cells with Front Nanobowl Texture and Truncated-Nanopyramid Reflector. *Opt. Lett.* **2015**, *40*, 1077−1080.
(23) Yang, Z.; Shang, A.; Qin, L.; Zhan, Y.; Zhang, C.; Gao, P.; Ye, J.; Li, X. Broadband and Wide-Angle Light Harvesting by Ultra-Thin Silicon Solar Cells with Partially Embedded Dielectric Spheres. *Opt. Lett.* **2016**, *41*, 1329−1332.
(24) Gao, P.; Wang, H.; Sun, Z.; Han, W.; Li, J.; Ye, J. Efficient Light Trapping in Low Aspect-Ratio Honeycomb Nanobowl Surface Texturing for Crystalline Silicon Solar Cell Applications. *Appl. Phys. Lett.* **2013**, *103*, 253105.
(25) Gao, P.; He, J.; Zhou, S.; Yang, X.; Li, S.; Sheng, J.; Wang, D.; Yu, T.; Ye, J.; Cui, Y. Large-Area Nanosphere Self-Assembly by a Micro-Propulsive Injection Method for High Throughput Periodic Surface Nanotexturing. *Nano Lett.* **2015**, *15*, 4591−4598.
(26) Schmidt, J.; Titova, V.; Zielke, D. Organic-Silicon Heterojunction Solar Cells: Open-Circuit Voltage Potential and Stability. *Appl. Phys. Lett.* **2013**, *103*, 183901.
(27) Jäckle, S.; Mattiza, M.; Liebhaber, M.; Brönstrup, G.; Rommel, M.; Lips, K.; Christiansen, S. Junction Formation and Current Transport Mechanisms in Hybrid n-Si/PEDOT:PSS Solar Cells. *Sci. Rep.* **2015**, *5*, 13008.
(28) Yu, X.; Shen, X.; Mu, X.; Zhang, J.; Sun, B.; Zeng, L.; Yang, L.; Wu, Y.; He, H.; Yang, D. High Efficiency Organic/Silicon-Nanowire Hybrid Solar Cells: Significance of Strong Inversion Layer. *Sci. Rep.* **2015**, *5*, 17371.
(29) Erickson, A. S.; Zohar, A.; Cahen, D. n-Si−Organic Inversion Layer Interfaces: A Low Temperature Deposition Method for Forming a p−n Homojunction in n-Si. *Adv. Energy Mater.* **2014**, *4*, 1301724.
(30) Karakasoglu, I.; Wang, K. X.; Fan, S. Optical-Electronic Analysis of the Intrinsic Behaviors of Nanostructured Ultrathin Crystalline Silicon Solar Cells. *ACS Photonics* **2015**, *2*, 883−889.
(31) Zhang, X.; Yang, D.; Yang, Z.; Guo, X.; Liu, B.; Ren, X.; Liu, S. Improved PEDOT:PSS/c-Si Hybrid Solar Cell Using Inverted Structure and Effective Passivation. *Sci. Rep.* **2016**, *6*, 35091.
(32) Yang, L.; Liu, Y.; Chen, W.; Wang, Y.; Liang, H.; Mei, Z.; Kuznetsov, A.; Du, X. Interface Engineering of High Efficiency Organic-Silicon Heterojunction Solar Cells. *ACS Appl. Mater. Interfaces* **2016**, *8*, 26−30.
(33) Dai, X.; Chen, T.; Cai, H.; Wen, H.; Sun, Y. Improving Performance of Organic-Silicon Heterojunction Solar Cells Based on Textured Surface via Acid Processing. *ACS Appl. Mater. Interfaces* **2016**, *8*, 14572−14577.
(34) Savagatrup, S.; Chan, E.; Renteria-Garcia, S. M.; Printz, A. D.; Zaretski, A. V.; O'Connor, T. F.; Rodriquez, D.; Valle, E.; Lipomi, D. J. Plasticization of PEDOT:PSS by Common Additives for Mechanically Robust Organic Solar Cells and Wearable Sensors. *Adv. Funct. Mater.* **2015**, *25*, 427−436.
(35) Yang, Z.; Shang, A.; Zhan, Y.; Zhang, C.; Li, X. Ultra-Broadband Performance Enhancement of Thin-Film Amorphous Silicon Solar Cells with Conformal zig−zag Configuration. *Opt. Lett.* **2013**, *38*, 5071−5074.
(36) Yang, Z.; Gao, P.; Zhang, C.; Li, X.; Ye, J. Scattering Effect of the High-Index Dielectric Nanospheres for High Performance Hydrogenated Amorphous Silicon Thin-Film Solar Cells. *Sci. Rep.* **2016**, *6*, 30503.
(37) Li, X.; Hylton, N.; Giannini, V.; Lee, K. H.; Ekins-Daukes, N. J.; Maier, S. A. Multi-Dimensional Modeling of Solar Cells with Electromagnetic and Carrier Transport Calculations. *Prog. Photovoltaics* **2013**, *21*, 109−120.

DOI: 10.1021/acsenergylett.7b00015
ACS Energy Lett. 2017, 2, 556−562